Density data for carbon dioxide (CO2) +trans-1,3,3,3-tetrafluoroprop-1-ene (R-1234ze(E)) mixture at temperatures from 283.32 to 353.02K and pressures up to 10MPa

Yuxin Fu, Alain Valtz, Snaïde Ahamada, Haitao Hu, Christophe Coquelet

Density data for carbon dioxide (CO_2) +trans-1,3,3,3-tetrafluoroprop-1-ene (R-1234ze(E)) mixture at temperatures from 283.32 to 353.02K and pressures up to 10 MPa

Yuxin FU[1], Alain VALTZ[2], Snaïde AHAMADA[2], Haitao HU[1], Christophe COQUELET[2]
1 Institute of Refrigeration and Cryogenics, Shanghai Jiao Tong Univ, 800 Dongchuan Rd, 200240 Shanghai, China
2 Mines ParisTech, PSL University, CTP – Centre of Thermodynamics of Processes 35, rue Saint Honoré 77305 Fontainebleau Cedex France

ABSTRACT

The densities of CO_2-R1234ze(E) (trans-1,3,3,3-tetrafluoroprop-1-ene) binary mixture were measured using VTD densitometer, Anton Paar DMA 512, in the gas, liquid and supercritical phases. Four compositions of mixtures: 21.3% CO_2+ 78.7% R1234ze(E), 40% CO_2+ 60% R1234ze(E), 59.6% CO_2+ 40.6% R1234ze(E) and 79.4% CO_2+ 20.6% R1234ze(E) were studied at seven temperatures between 283.32K and 353.02K and pressures up to 10MPa. The data were well correlated using the Peng-Robinson cubic equation of State using the Wong Sandler mixing rules involving the NRTL activity coefficient model, and the fundamental Helmholtz equation of state using the Kunz and Wagner mixing rules involving Helmholtz energy. The experimental and correlated phase compositions were compared. Both two models were adjusted on the VLE data, but the Helmholtz model is more accurate to the prediction of density than the Peng-Robinson model.

Key words:CO_2 and R1234ze(E) mixture, Thermodynamic properties prediction model, Vibrating tube densitometer, Monophasic condition, Binary interaction parameters

NOMENCLATURE

a	Cohesive energy parameter (J m^3 mol^{-2})
b	Covolume parameter (m^3 mol^{-1})
c	Exponent of reduced Helmholtz free energy
CFC	Chlorofluorocarbon
COP	Coefficient of Performance
d	Exponent of reduced Helmholtz free energy
EoS	Equation of state
F	Departure function
g	Molar Gibbs energy (J.mol^{-1})
HCFC	Hydro chlorofluorocarbon
HFC	Hydro fluorocarbon
k_{ij}	Binary interaction parameter (BIP)
K	Potential energy parameter/integer of reduced Helmholtz energy
MRD	Mean relative deviation
N	Number of experimental data point
n	Coefficient of reduced Helmholtz energy
ODP	Ozone depletion potential
OF	Objective function
P	Pressure (MPa) / 1MPa = 10^6 Pa
PR	Peng-Robinson
R	Gas constant (J mol^{-1} K^{-1})
S	Entropy
t	Exponent of reduced Helmholtz free energy
T	Temperature (K)
u	Uncertainty
v	Molar volume (m^3 mol^{-1})
VCC	Volumetric Cooling Capacity
VLCC	vapor-liquid coexistence curve
VTD	Vibrating Tube Densitometer
x	Liquid mole fraction
y	Vapor mole fraction
Z	Compressibility factor

HFOs	Hydrofluoroolefins
GWP	Global warming potential

Greek letters

α	NRTL non randomness parameter or reduced Helmholtz energy
β	Binary interaction parameter for Helmholtz EoS/ exponent of departure function part of reduced Helmholtz energy
γ	Binary interaction parameter for Helmholtz EoS/ exponent of departure function part of reduced Helmholtz energy
ε	Exponent of departure function part of reduced Helmholtz energy
η	Exponent of departure function part of reduced Helmholtz energy
ω	Acentric factor
θ	Parameter of ideal part of reduced Helmholtz energy
φ	Fugacity
μ	Chemical potential
ρ	Molar density (mol m^{-3})
τ	NRTL parameter ($J.mol^{-1}$)/inverse reduced temperature

Subscripts

c	Critical property
0	Reference state
cal	Calculated property
exp	Experimental property
i,j	Molecular species
k	Number of parameters, coefficients and exponents for reduced Helmholtz energy
r	Reference

Superscripts

V	Vapor phase
L	Liquid phase
E	Excess property
0	Ideal part
r	Residual part

1 Introduction

Atmospheric greenhouse effect, stratospheric ozone depletion and acid rain are three major environmental hazards across the globe. Ozone depletion potential (ODP) and global warming potential (GWP) become the two main standards to evaluate the performance of a refrigerant. However, in general, refrigerants such as chlorofluorocarbons (CFCs) and hydro chlorofluorocarbons (HCFCs) have high ODP while hydro fluorocarbons (HFCs) have high GWP.

Therefore, in 1987, the Montreal Protocol proposed that those refrigerants with high ODP should be replaced and eliminated by an environmentally friendly one to protect the ozonosphere (United Nations [1]). In 1998, the Kyoto Protocol to the United Nations proposed that all the countries participating in this protocol should take in charge of limiting greenhouse gas emissions (United Nations [2]). In 2014, a F-gas regulation in Europe is created to fix the limit of utilization of the total amount of the most important fluorinated greenhouse gases (F-gases), to ban the use of high GWP fluorinated compound in many new types of equipment, and preventing emissions of F-gases from existing equipment (Anonymous [3]). In October 2016, the parties of Montreal Protocol reached an agreement to phase-down HFCs during the meeting in Kigali (UNEP [4]).

Besides the ODP and GWP, the ideal refrigerant should also meet those standards: high diathermancy, high mobility, high chemical and thermal durability, no toxicity, no flammability and suitable thermodynamic and volumetric properties in the refrigeration system.

To find out a suitable refrigerant with low ODP and low GWP, the optimal composition of refrigerant, and an accurate thermodynamic model, some researches on thermodynamic properties have been done.

In recent years, R1234ze (E) (trans-1,3,3,3-tetrafluoroprop-1-ene) is considered as the next generation refrigerants for its zero ODP and low GWP (GWP<1). However, because of its low latent heat of vaporization and slightly low evaporation pressure, its Coefficient of

Performance (COP) and Volumetric Cooling Capacity (VCC) is relatively smaller than usual refrigerants such as R134a and R410a (Qiu et al.[5]).

Carbon dioxide (CO_2) was once used as an important refrigerant for half a century. After 1930, the widespread use of CFCs refrigerants eliminated CO_2. As the current CFCs are eliminated, it is revalued and reapplied. It has ODP=0, GWP=1 (3260 times smaller than that of R404a), safety level A1, at the same time, it is a natural fluid. Those properties enable it to replace CFCs and HCFCs. Its other advantages are: the cooling capacity is 5 times larger than R22; the pressure ratio of the compressor is small; the heat transfer performance is good; the relative pressure loss during flow is small. However, its critical temperature is around 31°C, which is relatively small (Wu [6]).

Therefore, the idea of utilization of refrigerant mixtures has been proposed to increase the cycle efficiency and adjust the environment of refrigeration and obtain a coherent temperature glide. Currently, some of the most promising refrigerant mixtures are composed of R1234yf or R1234ze(E) with HFC or natural refrigerants.

The mixture CO_2 + R1234ze(E) systems have been researched from different aspects. In 2014, the critical loci of CO_2 + R1234ze(E) were measured over the whole composition range (Juntarachat [7]). In 2017, the P-x-y VLE data of CO_2 and R1234ze(E) mixture have been measured at temperatures ranging from 283.32 to 353.02 K and pressures up to 7.6 MPa (Wang et al.[8]). In 2018, P-ρ and T-ρ VLE diagrams of four mixtures of CO_2 + R1234ze(E) with different compositions (mole fraction % (20/80), (40/60), (60/40), (80/20)) have already been established, at the vicinity of critical point (Xie et al. [9]).

However, the database of new refrigerant is still rare, especially the P-ρ diagrams out of VLE for the different mixtures. In general, the strategy of selection of a working fluid is to compare experimental values with the calculated densities and equilibrium properties (VLE), then the enthalpy and finally the COP. Then, if model predictions are not very good, the next step is the optimization of model's parameters that can predict other data that isn't measured.

In this work, four mixtures of CO_2+R-1234ze(E) (in mole %: (20/80), (40/60), (60/40) and (80/20) with different compositions (%) were prepared. Measurements are done at a constant temperature. For each mixture, four temperatures between the seven temperatures

among (283.32 K, 293.15 K and 298.15 K below the critical temperature of CO_2, 308.13 K, 318.11 K, 333.01 K and 353.02 K above) are selected. Density measurements were performed using a vibrating tube densitometer: temperature pressure and period of vibration of the tube were recorded. Calibration must be realized to link density and period of vibration and CO_2, as reference fluid, is considered.

Experimental data will be fitted into Matlab® environment using Fundamental Helmholtz equation of state by adjustment of the binary interaction parameters. Comparisons will be done with Peng-Robinson equation of state predictions developed by Wang et al. [8].

2 Experimental part

2.1. Materials

CO_2 and R-1234ze(E) were purchased from Air Liquide and Honeywell with a purity higher than 99.995 vol.% and 99 vol.% (Table 1) respectively. Table 2 presents the exact composition of the 4 mixtures. The composition was determined after successive weighing (Wi) of empty recipient, W_1, recipient with R1234ze(E), W_2 and recipient with R-1234ze(E) and CO_2,W_3. Consequently, $m_{R1234ze(E)} = W_2 - W_1$ and $m_{CO_2} = W_3 - W_2$. Considering molar mass, one can calculate the R-1234ze(E) composition: $z_{R-1234ze(E)} = \frac{\frac{m_{R-1234ze(E)}}{M_{R-1234ze(E)}}}{\frac{m_{R-1234ze(E)}}{M_{R-1234ze(E)}}+\frac{m_{CO_2}}{M_{CO_2}}}$.

The uncertainty of molar fractions is determined by the equation (1):

$$u(x_1) = x_1(1-x_1)\sqrt{\frac{u(W_1)^2}{W_1} + \frac{u(W_2)^2}{W_2} + \frac{u(W_3)^2}{W_3}} \quad (1)$$

With $u(W_i) = \frac{a}{\sqrt{3}}$ where a is the accuracy of the mass balance (a=±0.0001g).

[Table 1]

Table 1: Chemical samples used for experimental work.

Chemicals	CAS number	Supplier	Purity (vol %)	Analysis method[a]
CO_2	124-38-9	Air Liquide	99.995	GC
R-1234ze(E)	29118-24-9	Honeywell	99	GC

[a] GC: Gas Chromatography

[Table 2]

Table 2: Expected composition and real composition mole fractions.

Expected composition mole fractions		Real composition mole fractions		Uncertainties $U(x_1)$
CO_2	R1234ze(E)	CO_2	R1234ze(E)	
0.2	0.8	0.21263	0.78737	10^{-5}
0.4	0.6	0.40016	0.59984	10^{-5}
0.6	0.4	0.59632	0.40368	10^{-5}
0.8	0.2	0.79409	0.20591	10^{-5}

2.2. Apparatus

The Vibrating Tube Densitometer (VTD), Anton Paar DMA HPM was used to measure the densities. This equipment is similar to that described by Coquelet et al. [10] or Nazeri et al. [11]. A schematic diagram of the apparatus used is presented in figure 1.

[Figure 1]

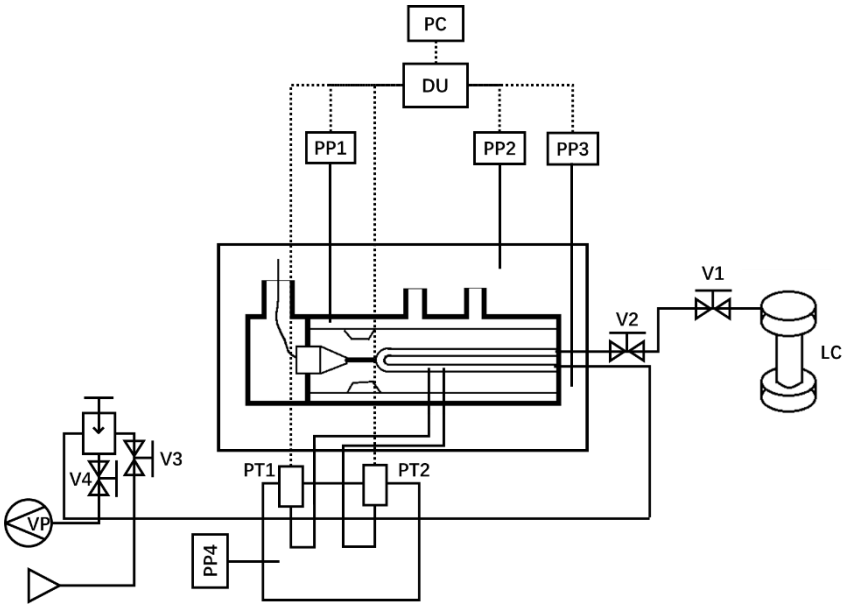

Figure 1 Schematic diagram of pressure and density measurement apparatus. LC: loading cell; V: valve; PP: platinum probe; PT: pressure transducer; PC: personal computer; VP: vacuum pump; DU: data acquisition; Full line: tube; Dotted line: electric wire

Briefly, the main part of the setup is the U-shaped vibrating tube Anton Paar densitometer. Its operating pressure up to 140 MPa and its temperature range is within 263 – 473 K. The tube material is made of Hastelloy. The temperature is controlled by fluid that circulates in a jacket (small liquid bath) around the densitometer. The temperature stability is of ±0.02 K.

The sample fluid is introduced from the loading cell into the densitometer through the tube with the diameter of 1.6 mm (1/16 inches). The whole connection tubes are fully immersed in the temperature controlled liquid bath model West P6100. Four-wire 100-Ω platinum resistance probes (Pt100) (PP) measure the temperature at each part of the equipment. The PP were calibrated against the reference thermometer with 25-Ω (model: Tinsley Precision Instrument). The standard uncertainty of the temperature probes were estimated to be $u(T)$ = 0.08 K after calibration. There are two pressure transducers (PT) of type PAA-35HXTC to measure different levels of pressure. PT1 can measure the pressure up to 3MPa, and PT2 can measure the pressure up to 70MPa. The transducers were calibrated with an electronic balance (model: GE Sensing PACE 5000) at pressure up to 20 MPa and using a dead weight tester (model: Desgranges & Huot 5202S) for pressures from 20 to 40 MPa.

The pressure transducers can measure the pressure with the standard uncertainties of *u(p)* = 0.002 MPa and *u(p)* = 0.005 MPa in the ranges of 0-3 MPa and 3-10 MPa, respectively. The pressure and the temperature were recorded using Agilent HP34970A data acquisition unit and the vibration period, τ, also was recorded using a HP53131A data acquisition unit. The calibration will be realized by using a common fluid CO_2. The relation between the pressure and the density of CO_2 is given by REFPROP™ 10.0 [12].

2.3. Calibration and Experimental procedure

The densitometer was firstly calibrated using pure CO_2 and forced path mechanical calibration (FPMC) model [13 - 14 -15]. The density data from Span and Wagner EoS, implemented in REFPROP 10.0 software [16] were used to tune the unknown parameters in this model at full ranges of pressures for each measured isotherm. The measurement procedure is well described in previous publication (Coquelet et al. [10], Nazeri et al. [17]). It can be noticed that before the appearance of dew point, the temperature of liquid bath should be slightly higher than that of the jacket (around the vibrating tube) (difference about 0.2-0.3°C), to make sure that the first drop of refrigerant appears exactly in the densitometer. Also, before the appearance of bubble point, the temperature of liquid bath should be slightly low than that of the jacket (around the vibrating tube) (difference about 0.2-0.3°C) to make sure that the first bubble of refrigerant appears exactly in the densitometer.

The uncertainties of densities are therefore calculated using Eq. (2) taking into account the calibration with the reference fluid, i.e. carbon dioxide. Measurements are realized at constant temperature and the temperature contribution to the density uncertainty is not considered.

$$u(\rho) = \sqrt{\left(\frac{\alpha}{\sqrt{3}}\right)^2 + \left(\frac{\partial \rho_{CO_2}}{\partial P}\right)^2 \left(u(P)\right)^2} \qquad (2)$$

In Eq. 2, α represents the maximum of absolute deviations ($\left|\rho_{cal} - \rho_{exp}\right|$) between the experimental CO_2 densities (reference fluid) and that calculated by REFPROP 10.0 at the

same conditions of T and P. $\frac{\partial \rho_{CO_2}}{\partial P}$, the derivative of carbon dioxide density with respect to pressure, is calculated by REFPROP 10.0. As the compressibility depend on the temperature, the density and the pressure, the uncertainties of the compressibility are therefore expressed using the Eq. (3):

$$u(Z) = Z\sqrt{\left(\frac{u(\rho)}{\rho}\right)^2 + \left(\frac{u(T)}{T}\right)^2 + \left(\frac{u(P)}{P}\right)^2} \quad (3)$$

3 Correlation

Two models will be used to correlate the new experimental data.

The first one is the model developed by Wang et al. [8]. The critical temperatures (Tc), critical pressures (Pc) and acentric factors of each pure compound are taken from the REFPROP 10.0 and presented in Table 3.

[Table 3]

Table 3: Critical parameters and acentric factors of CO_2 and R-1234ze(E) from REFPROP 10.0 [12].

Compound	T_c (K)	P_c (MPa)	Acentric factor (ω)
CO_2	304.13	7.377	0.224
R-1234ze(E)	382.51	3.635	0.313

The model developed by Wang et al. [8] consists of the Peng-Robinson cubic Equation of State (PR EoS) (1978) [18], the Wong-Sandler (WS) mixing rules (Eqs. (4) ~ (7)) [19] and the NRTL local composition model (Eq. (8)) [20] as excess Gibbs energy model.

$$\left(P + \frac{a(T)}{(v^2 + 2bv - b^2)}\right)(v - b) = RT \quad (4)$$

With $a = \Omega_a \frac{R^2 T_C^2}{P_C}$, $b = \Omega_b \frac{RT_C}{P_C}$, $\Omega_a = 0.457240$, $\Omega_b = 0.07780$

And $a(T)=a_C\alpha(T)$, $\alpha(T)=\left[1+m\left(1-T_R^{1/2}\right)\right]^2$ with $m=0.374640+1.542260\omega-0.26992\omega^2$.

$$b=\frac{\sum_i\sum_j x_i x_j\left(b-\frac{a}{RT}\right)_{ij}}{1-\left(\frac{\sum_i x_i\frac{a_i}{b_i}}{RT}+\frac{g^E(T,P=\infty,x_i)}{CRT}\right)} \quad (5)$$

$$b-\frac{a}{RT}=\sum_i\sum_j x_i x_j\left(b-\frac{a}{RT}\right)_{ij} \quad (6)$$

$$\left(b-\frac{a}{RT}\right)_{ij}=\frac{1}{2}\left[\left(b-\frac{a}{RT}\right)_i+\left(b-\frac{a}{RT}\right)_j\right](1-k_{ij}) \quad (7)$$

k_{ij} is a binary interaction parameter and $C=\ln(1/2)$.

$$\frac{g^E(T,P,x_1)}{RT}=\sum_i x_i\sum_j\frac{x_j\exp\left(-\alpha_{ji}\frac{\tau_{ji}}{RT}\right)}{\sum_k x_k\exp\left(-\alpha_{ki}\frac{\tau_{ki}}{RT}\right)}\tau_{ji} \quad (8)$$

with $\tau_{ii}=0$ and $\alpha_{ii}=0$. α_{ji}, τ_{ji} ($\neq\tau_{ij}$) are adjustable parameters and $\alpha_{ji}=0.3$. The adjusted parameters are presented in Table 4.

[Table 4]

Table 4: Values of the binary interaction parameters from Wang et al. [8] at each temperature.

T/ K	τ_{12}/ J.mol^{-1}	τ_{21}/ J.mol^{-1}	k_{12}
283.32	-8.264	287.3	0.2546
293.15	-2128	3492	0.2350
298.15	-1495	2321	0.2336
308.13	-2339	3568	0.2814
318.11	-2388	3667	0.2709
333.01	-441	693	0.2715
353.02	-36.71	511	0.2909

The second model is of Helmholtz type Eos. All the thermodynamics properties can be determined by derivation of Helmholtz energy. Fundamental Helmholtz EoS are used in REFPROP10.0 to calculate the mixture thermodynamic properties. The definition of Helmholtz energy is given by Eq. 9.

$$dA=-SdT-pdV+\sum_{i=1}^{N}\mu_i dn_i \quad (9)$$

where A is the Helmholtz energy, S is the entropy, μ_i is the chemical potential of component i, and N is the number of components. For each component, the reduced Helmholtz energy α depending on the temperature and the molar density is defined by Eq. 10 (Kunz and Wagner [21]).

$$\alpha(T,\rho) = \frac{\mathrm{A}(T,\rho)}{RT} = \alpha_0^0(T,\rho) + \alpha_0^r(\tau,\delta) \tag{10}$$

where A represents the molar Helmholtz energy, $\alpha_0^0(T,\rho)$ represents the ideal part, and $\alpha_0^r(\tau,\delta)$ represents the residual part. δ is the reduced density and τ is the reduced temperature defined by $\delta = \frac{\rho}{\rho_c}$ and $\tau = \frac{T_c}{T}$ with ρ_c the molar critical density and T_c the critical temperature. The equation of ideal part is given by Eq. 11.

$$\alpha_0^0(T,\rho) =$$
$$\ln\left(\frac{\rho}{\rho_c}\right) + \frac{R^*}{R}\left[n_{0,1}^0 + n_{0,2}^0\frac{T_c}{T} + n_{0,3}^0 \ln\left(\frac{T_c}{T}\right) + \sum_{k=4,6} n_{0,k}^0 \ln\left(\left|\sinh\left(\theta_{0,k}^0\frac{T_c}{T}\right)\right|\right) -\right.$$
$$\left.\sum_{k=5,7} n_{0,k}^0 \ln\left(\cosh\left(\theta_{0,k}^0\frac{T_c}{T}\right)\right)\right] \tag{11}$$

where $n_{0,k}^0$and $\theta_{0,k}^0$are series of parameters given. The equation of residual part is given by Eq. 12.

$$\alpha_0^r(\tau,\delta) =$$
$$\sum_{k=1}^{K_{pol}} n_{0,k}\,\delta^{d_{0,k}}\tau^{t_{0,k}} + \sum_{k=K_{pol}+1}^{K_{pol}+K_{exp}} n_{0,k}\delta^{d_{0,k}}\tau^{t_{0,k}}\exp(-\delta^{c_{0,k}}) +$$
$$\sum_{k=K_{pol}+1}^{K_{pol}+K_{exp}+K_{expp}} n_{0,k}\delta^{d_{0,k}}\tau^{t_{0,k}}\exp\left(-\eta_{0,k}\left(\delta-\varepsilon_{0,k}\right)^2 - \beta_{0,k}\left(\tau-\gamma_{0,k}\right)^2\right) \tag{12}$$

where $n_{0,k}, d_{0,k}, t_{0,k}$ and $c_{0,k}$are series of parameters given, K_{pol}, K_{exp} and K_{expp} are three integers given. For a mixture, the reduced Helmholtz energy is defined by Eq. 13.

$$\alpha(T,\rho,\bar{x}) = \alpha^0(T,\rho,\bar{x}) + \alpha^r(\tau,\delta,\bar{x}) \tag{13}$$

where $\bar{x}$ represents the molar fraction, $\delta = \frac{\rho}{\rho_r(\bar{x})}$ and $\tau = \frac{T_r(\bar{x})}{T}$. $\rho_r(\bar{x})$ represents the reference density, and $T_r(\bar{x})$ represents the reference temperature, as shown in Eqs. 14 and 15.

$$\frac{1}{\rho_r(\bar{x})} = \sum_{i=1}^{N} x_i^2 \frac{1}{\rho_{c,i}} + \sum_{i=1}^{N-1}\sum_{j=i+1}^{N} 2x_i x_j \beta_{v,ij}\gamma_{v,ij}\frac{x_i+x_j}{\beta_{v,ij}{}^2 x_i + x_j}\cdot\frac{1}{8}\left(\frac{1}{\rho_{c,i}^{\frac{1}{3}}} + \frac{1}{\rho_{c,j}^{\frac{1}{3}}}\right)^3 =$$

$$\sum_{i=1}^{N} x_i^2 \frac{1}{\rho_{c,i}} + \sum_{i=1}^{N-1} \sum_{j=i+1}^{N} c_{v,ij} f_{v,ij}(x_i, x_j)$$

(14)

with $c_{v,ij} = 2\beta_{v,ij}\gamma_{v,ij} \cdot \frac{1}{8}\left(\frac{1}{\rho_{c,i}^{\frac{1}{3}}} + \frac{1}{\rho_{c,j}^{\frac{1}{3}}}\right)^3 f_{v,ij}(x_i, x_j) = x_i x_j \frac{x_i + x_j}{\beta_{v,ij}^{\ 2} x_i + x_j}$

$$T_r(\overline{x}) = \sum_{i=1}^{N} x_i^2 T_{c,i} + \sum_{i=1}^{N-1} \sum_{j=i+1}^{N} c_{T,ij} f_{T,ij}(x_i, x_j) \quad (15)$$

with $c_{T,ij} = 2\beta_{T,ij}\gamma_{T,ij} \cdot (T_{c,i} \cdot T_{c,j})^{0.5} f_{T,ij}(x_i, x_j) = x_i x_j \frac{x_i + x_j}{\beta_{T,ij}^{\ 2} x_i + x_j}$ where $\beta_{v,ij}$, $\gamma_{v,ij}$, $\beta_{T,ij}$ and $\gamma_{T,ij}$ are reducing function parameters adjusted by VLE experimental data.

The ideal part of the reduced Helmholtz energy depends on that of each component and their molar fraction Eq. 16.

$$\alpha^0(T, \rho, \bar{x}) = \sum_{i=1}^{N} x_i [\alpha_{0i}^0(T, \rho) + \ln(x_i)] \quad (16)$$

The residual part depends besides the residual part of component, the empirical multi-parameters function Eq. (16).

$$\alpha^r(\tau, \delta, \bar{x}) = \sum_{i=1}^{N} x_i \alpha_{0i}^r(\tau, \delta) + \sum_{i=1}^{N-1} \sum_{j=i+1}^{N} x_i x_j F_{ij} \alpha_{ij}^r(\tau, \delta) \quad (17)$$

where $F_{ij}$is the binary parameter between each two components, and $\alpha_{ij}^r(\tau, \delta)$the departure function of two components, as calculated by Eq. 18.

$$\alpha_{ij}^r(\tau, \delta) = \sum_{k=1}^{K_{pol,ij}} n_{ij,k} \delta^{d_{ij,k}} \tau^{t_{ij,k}} + \sum_{k=K_{pol,ij}+1}^{K_{pol,ij}+K_{exp,ij}} n_{ij,k} \delta^{d_{ij,k}} \tau^{t_{ij,k}} \cdot \exp\left(-\eta_{ij,k}(\delta - \varepsilon_{ij,k})^2 - \beta_{ij,k}(\delta - \gamma ij,k\right) \quad (18)$$

with $n_{ij,k}$, $d_{ij,k}$, $t_{ij,k}$, $\eta_{ij,k}$, $\varepsilon_{ij,k}$, $\gamma_{ij,k}$, $K_{pol,ij}$ and $K_{exp,ij}$parameters of interaction.

In this correlation, F_{ij} is defined as 0, and the departure function isn't taken into account in this model.

The parameters for each pure component is presented in Table 5

[Table 5]

Table 5: Values of parameters of CO_2 [16] and R1234ze(E) [22] for Helmholtz EoS

k	$n_{0i,k}$	$d_{oi,k}$	$t_{oi,k}$	$c_{oi,k}$
		CO_2		
1	0.388568	1	0	
2	2.938548	1	0.75	
3	-5.586719	1	1	
4	-0.767532	1	2	
5	0.31729	2	0.75	
6	0.548033	2	2	
7	0.122794	3	0.75	
8	2.165896	1	1.5	1
9	1.584174	2	1.5	1
10	-0.231327	4	2.5	1
11	0.058117	5	0	1
12	-0.553691	5	1.5	1
13	0.489466	5	2	1
14	-0.024276	6	0	1
15	0.062495	6	1	1
16	-0.121759	6	2	1
17	-0.370557	1	3	2
18	-0.016776	1	6	2
19	-0.119607	4	3	2
20	-0.045619	4	6	2
21	0.035613	4	8	2
22	-0.007443	7	6	2
23	-0.00174	8	0	2
24	-0.02181	2	7	3
25	0.024332	3	12	3
26	-0.03744	3	16	3
27	0.143387	5	22	4
28	-0.13492	5	24	4
29	-0.023151	6	16	4
30	0.012363	7	24	4
31	0.002106	8	8	4
32	-0.00034	10	2	4
33	0.005599	4	28	5
34	-0.000303	8	14	6
		R1234ze(E)		
1	0.039828	4	1	
2	1.812227	1	0.223	
3	-2.537512	1	0.755	
4	-0.533325	2	1.24	

5	0.167703	3	0.44	
6	-1.323801	1	2	2
7	-0.669465	3	2.2	2
8	0.807272	2	1.2	1
9	-0.774023	2	1.5	2
10	-0.018438	7	0.9	1

*$K_{pol,CO2}$=7, $K_{exp,CO2}$=27, $K_{pol,R1234ze(E)}$=5, $K_{exp,R1234ze(E)}$=5.

By the definition of Helmholtz energy, some of the thermodynamic properties can be calculated by the derivation.

- Calculation of the pressure P (Eq. 19).

By definition, $p(T,\rho,\bar{x}) = -\left(\frac{\partial A}{\partial v}\right)_{T,\bar{x}} = -RT\left(\frac{\partial \alpha}{\partial v}\right)_{T,\bar{x}} = \delta\rho RT\left(\frac{\partial \alpha}{\partial \delta}\right)_{T,\bar{x}}$ and so, $\frac{p(T,\rho,\bar{x})}{\rho RT} = \delta\left(\left(\frac{\partial \alpha^0}{\partial \delta}\right)_{T,\bar{x}} +$ $\partial ar\partial\delta T,x=\delta i=1Nxi\partial a0i0\partial\delta T,x+\delta a\delta r$

$$\frac{p(T,\rho,\bar{x})}{\rho RT} = 1 + \delta\alpha_\delta^r \quad (19)$$

- Calculation of the fugacity for each component:

By definition, $\ln(\varphi_i) = \left(\frac{\partial n\alpha^r}{\partial n_i}\right)_{T,V,n_j} - \ln(1+\delta\alpha_\delta^r)$. For the residual part $\left(\frac{\partial n\alpha^r}{\partial n_i}\right)_{T,V,n_j}$, the calculation is given by Eq. 20.

$n\left(\frac{\partial \alpha^r}{\partial n_i}\right)_{T,V,n_j} = \delta\alpha_\delta^r\left[1 - \frac{1}{\rho_r}\cdot n\left(\frac{\partial \rho_r}{\partial n_i}\right)_{n_j}\right] + \tau\alpha_\tau^r\frac{1}{T_r}\cdot n\left(\frac{\partial T_r}{\partial n_i}\right)_{n_j} + \alpha_{x_i}^r - \sum_{k=1}^{N} x_k\,\alpha_{x_k}^r$ and $\left(\frac{\partial n\alpha^r}{\partial n_i}\right)_{T,V,n_j} =$ $\alpha^r + n\left(\frac{\partial \alpha^r}{\partial n_i}\right)_{T,V,n_j}$ (20)

Eq. 21 is considered for the initialization of binary interaction parameters (Stefan Herrigaus Essen [23]).

$$\beta_{T,ij} = 1\;\gamma_{T,ij} = \frac{1}{2}\frac{T_{c,i}+T_{c,j}}{(T_{c,i}T_{c,j})^{0.5}}\;\beta_{v,ij} = 1\;\gamma_{v,ij} = 4\frac{\frac{1}{\rho_{c,i}}+\frac{1}{\rho_{c,j}}}{(\frac{1}{\rho_{c,i}^{\frac{1}{3}}}+\frac{1}{\rho_{c,j}^{\frac{1}{3}}})^3} \quad (21)$$

Binary interaction parameters β_T and γ_T are adjusted using Matlab®, based on the

experimental data of bubble point pressure and the composition of vapor phase obtained by Wang et al. [8], using a bubble pressure algorithm and Eq. 22 following objective function of minimization.

$$OF1 = \frac{1}{N_{data}-2}\sqrt{\sum_1^{N_{data}}\left(\frac{P_{exp}-P_{cal}}{P_{exp}}\right)^2 + \sum_1^{N_{data}}\left(\frac{y_{exp}-y_{cal}}{y_{exp}}\right)^2} \quad (22)$$

where N_{data} represents the number of experimental data points. P_{exp} and y_{exp} are given by experimental data, $P_{cal}$and $y_{cal}$are calculated by Matlab® using Helmholtz equation.

The binary interaction parameters β_v, and γ_v are adjusted based on experimental data of the molar density obtained during the experiment while β_T and γ_T obtained by the previous adjustment for each temperature will be used to the adjustment.

The objective function of minimization is presented by Eq. 23.

$$OF2 = \frac{1}{N_{data}-1}\sqrt{\sum_1^{N_{data}}\left(\frac{\rho_{exp}-\rho_{cal}}{\rho_{exp}}\right)^2} \quad (23)$$

where N_{data}represents the number of experimental data points.ρ_{exp} is given by experimental data, $\rho_{cal}$is calculated by Matlab® in using Helmholtz equation.

4 Results and discussion

The experimental data are presented in Table 6. As it is shown in the Table 6, at a fixed composition, and a fixed pressure, as the temperature rises, the compressibility rises. At a fixed temperature, as the pressure rises, the compressibility of vapor phase decreases and that of liquid phase increases.

Comparisons are done with the predictions using the PR EoS model and presented on figure 2. It can be seen that, the predictions for the PR EoS are in good agreement with the experimental data, but some important deviations particularly for the liquid phase were observed. It justifies the utilization of Helmholtz equation of state.

[Table 6]

Table 6 Experimental isothermal density data for CO_2 +R1234ze(E) mixture system. U(T)=0.08° C, U(p)=0.002MPa if p<3MPa and U(p)=0.005MPa if p>3MPa.

Phase	p/MPa	ρ/mol.m^{-3}		Z
		Exp.	$u_c(\rho)$	
21.3% CO2 + 78.7% R1234ze(E)				
318.17 K				
Gas	0.228	86.2	3.1	1.00
Gas	0.411	162.0	3.1	0.96
Gas	0.621	257.2	3.1	0.91
Gas	0.866	359.8	3.1	0.91
Gas	1.033	450.3	3.1	0.87
Gas	1.121	496.1	3.1	0.85
Gas	1.207	564.7	3.1	0.81
Gas	1.302	758.9	3.1	0.65
Gas	1.342	789.3	3.1	0.64
Gas	1.411	810.8	3.1	0.66
Gas	1.456	817.9	3.1	0.67
Gas	1.480	821.2	3.1	0.68
Gas	1.513	827.7	3.1	0.69
Gas	1.544	851.1	3.1	0.69
Gas	1.577	855.9	3.1	0.70
Gas	1.599	881.1	3.1	0.69
Gas	1.620	882.7	3.1	0.69
Liquid	2.370	10578.2	3.1	0.08
Liquid	2.372	10579.3	3.1	0.08
Liquid	2.571	10597.0	3.1	0.09
Liquid	2.571	10596.8	3.1	0.09
Liquid	2.733	10613.1	3.1	0.10
Liquid	2.882	10625.8	3.1	0.10
Liquid	2.885	10626.5	3.1	0.10
Liquid	3.033	10639.8	3.1	0.11
Liquid	3.033	10639.4	3.1	0.11
Liquid	3.132	10648.8	3.1	0.11
Liquid	3.134	10648.4	3.1	0.11
Liquid	3.288	10662.7	3.1	0.12
Liquid	3.288	10662.9	3.1	0.12
Liquid	3.433	10675.1	3.1	0.12
Liquid	3.433	10674.3	3.2	0.12

Liquid	3.537	10683.6	3.2	0.13
Liquid	3.651	10693.1	3.2	0.13
Liquid	3.655	10693.4	3.1	0.13
Liquid	3.657	10693.6	3.1	0.13
Liquid	3.776	10704.7	3.7	0.13
Liquid	3.788	10704.6	3.1	0.13
Liquid	3.802	10706.0	3.2	0.13
Liquid	3.805	10706.4	3.1	0.13
Liquid	3.852	10710.0	3.2	0.14
Liquid	3.853	10710.3	3.1	0.14
Liquid	3.894	10713.7	3.1	0.14
Liquid	3.895	10713.8	3.1	0.14
Liquid	3.932	10716.0	3.1	0.14
Liquid	3.934	10716.2	3.1	0.14
Liquid	3.968	10719.8	3.1	0.14
Liquid	3.970	10719.9	3.1	0.14
Liquid	3.994	10721.2	3.1	0.14
Liquid	3.995	10721.3	3.1	0.14
Liquid	4.025	10725.0	3.2	0.14
Liquid	4.027	10724.7	3.1	0.14
Liquid	4.055	10726.4	3.1	0.14
Liquid	4.055	10725.9	3.1	0.14
Liquid	4.090	10730.2	3.2	0.14
Liquid	4.096	10731.6	3.1	0.14
Liquid	4.139	10733.8	3.2	0.15
Liquid	4.142	10733.9	3.1	0.15
Liquid	4.193	10738.2	3.2	0.15
Liquid	4.196	10738.6	3.2	0.15
Liquid	4.245	10742.7	3.1	0.15
Liquid	4.246	10742.4	3.1	0.15
Liquid	4.332	10749.5	3.1	0.15
Liquid	4.332	10749.2	3.1	0.15
Liquid	4.447	10758.8	3.1	0.16
Liquid	4.447	10759.0	3.1	0.16
Liquid	4.557	10767.0	3.1	0.16
Liquid	4.558	10767.4	3.2	0.16
Liquid	4.683	10776.9	3.2	0.16
Liquid	4.683	10777.1	3.2	0.16
Liquid	4.782	10785.2	3.2	0.17
Liquid	4.782	10784.8	3.1	0.17
Liquid	4.891	10794.0	3.1	0.17
Liquid	5.017	10804.3	3.2	0.18
Liquid	5.019	10804.8	3.2	0.18

Liquid	5.235	10820.2	3.2	0.18
Liquid	5.237	10819.9	3.1	0.18
Liquid	5.494	10840.9	3.2	0.19
Liquid	5.495	10840.7	3.1	0.19
Liquid	5.744	10857.9	3.1	0.20
Liquid	5.747	10858.4	3.2	0.20
Liquid	6.049	10881.0	3.3	0.21
Liquid	6.051	10881.0	3.2	0.21
Liquid	6.266	10896.0	3.2	0.22
Liquid	6.267	10896.2	3.2	0.22
Liquid	6.448	10907.7	3.2	0.22
Liquid	6.452	10908.5	3.2	0.22
Liquid	6.753	10929.3	3.4	0.23
Liquid	6.754	10930.0	3.3	0.23
Liquid	6.947	10943.3	3.4	0.24
Liquid	6.949	10943.2	3.3	0.24
Liquid	6.953	10943.5	3.4	0.24
Liquid	7.523	10981.7	3.5	0.26
Liquid	7.526	10981.5	3.3	0.26
Liquid	7.999	11012.4	4.2	0.27
Liquid	8.002	11012.5	3.4	0.27
Liquid	8.490	11043.5	3.3	0.29
Liquid	9.036	11077.4	4.6	0.31
Liquid	9.522	11106.7	5.6	0.32
Liquid	9.523	11106.4	4.1	0.32
Liquid	10.096	11140.3	4.0	0.34
		333.01 K		
Gas	0.206	79.1	2.6	0.94
Gas	0.811	326.8	2.6	0.90
Gas	1.036	417.5	2.7	0.90
Gas	1.219	536.7	2.6	0.82
Gas	1.413	625.8	2.6	0.82
Gas	1.617	777.3	2.6	0.75
Liquid	1.821	1024.6	2.6	0.64
Liquid	1.906	1046.9	2.6	0.66
Liquid	1.950	1060.2	2.6	0.66
Liquid	2.015	1098.3	2.6	0.66
Liquid	2.062	1130.8	2.6	0.66
Liquid	2.111	1144.8	2.6	0.67
Liquid	2.627	9837.4	2.6	0.10
Liquid	2.813	9865.6	2.7	0.10
Liquid	3.093	9905.6	2.6	0.11
Liquid	3.202	9921.0	2.7	0.12

Liquid	3.329	9938.3	2.6	0.12
Liquid	3.423	9951.6	2.7	0.12
Liquid	3.622	9978.2	2.6	0.13
Liquid	3.729	9992.6	2.6	0.13
Liquid	3.729	9992.6	2.6	0.13
Liquid	3.729	9992.6	2.6	0.13
Liquid	3.890	10013.2	2.6	0.14
Liquid	4.000	10027.1	2.6	0.14
Liquid	4.157	10046.0	2.6	0.15
Liquid	4.233	10054.8	2.6	0.15
Liquid	4.308	10064.0	2.6	0.15
Liquid	4.376	10072.3	2.6	0.16
Liquid	4.462	10082.8	2.7	0.16
Liquid	4.529	10092.1	2.7	0.16
Liquid	4.574	10097.4	2.6	0.16
Liquid	4.634	10103.9	2.7	0.17
Liquid	4.694	10110.9	2.6	0.17
Liquid	4.755	10117.5	2.6	0.17
Liquid	4.780	10120.7	2.7	0.17
Liquid	4.806	10123.8	2.6	0.17
Liquid	4.875	10129.6	2.7	0.17
Liquid	4.900	10136.9	2.7	0.17
Liquid	4.964	10144.6	2.7	0.18
Liquid	5.059	10155.4	2.8	0.18
Liquid	5.234	10174.4	2.7	0.19
Liquid	5.515	10204.1	2.7	0.20
Liquid	5.773	10231.6	2.8	0.20
Liquid	6.062	10260.7	2.7	0.21
Liquid	6.550	10309.9	2.7	0.23
Liquid	7.031	10355.5	2.8	0.25
Liquid	7.417	10391.0	2.8	0.26
Liquid	7.423	10391.1	2.8	0.26
Liquid	8.047	10443.6	2.7	0.28
Liquid	8.597	10490.8	3.1	0.30
Liquid	9.083	10529.2	2.9	0.31
Liquid	9.587	10568.5	2.9	0.33
Liquid	10.079	10605.3	2.7	0.34
		353.05 K		
Gas	0.451	154.1	2.7	1.00
Gas	0.623	221.5	2.7	0.96
Gas	0.851	322.9	2.7	0.90
Gas	1.144	444.2	2.8	0.88
Gas	1.506	610.3	2.7	0.84

Gas	2.184	1035.6	2.7	0.72
Gas	2.535	1435.3	2.7	0.60
Gas	2.959	1619.0	2.7	0.62
Liquid	3.511	8582.1	2.7	0.14
Liquid	3.535	8596.1	2.7	0.14
Liquid	3.548	8598.3	2.7	0.14
Liquid	3.640	8640.0	2.7	0.14
Liquid	3.739	8678.1	2.7	0.15
Liquid	3.854	8722.1	2.7	0.15
Liquid	4.048	8791.0	2.7	0.16
Liquid	4.203	8834.4	2.7	0.16
Liquid	4.480	8917.8	2.8	0.17
Liquid	4.679	8973.3	2.7	0.18
Liquid	4.803	9002.9	2.7	0.18
Liquid	4.803	9002.7	2.7	0.18
Liquid	5.000	9053.0	2.7	0.19
Liquid	5.046	9063.3	2.7	0.19
Liquid	5.094	9074.9	2.7	0.19
Liquid	5.120	9080.8	2.7	0.19
Liquid	5.158	9089.8	2.7	0.19
Liquid	5.200	9099.6	2.7	0.19
Liquid	5.259	9112.7	2.7	0.20
Liquid	5.313	9124.8	2.7	0.20
Liquid	5.416	9148.8	2.7	0.20
Liquid	5.564	9179.1	2.7	0.21
Liquid	6.008	9273.6	2.8	0.22
Liquid	6.541	9367.0	2.7	0.24
Liquid	7.067	9453.9	2.7	0.25
Liquid	7.535	9524.4	2.8	0.27
Liquid	8.010	9592.8	2.7	0.28
Liquid	8.538	9663.5	2.7	0.30
Liquid	9.030	9725.7	2.8	0.32
Liquid	9.543	9785.8	2.8	0.33
Liquid	9.745	9808.7	2.8	0.34
Liquid	10.070	9844.2	2.9	0.35
40.0% CO_2 + 60.0% R1234ze(E)				
283.09 K				
Gas	0.201	93.4	3.2	0.92
Gas	0.250	116.4	3.2	0.91
Gas	0.250	116.3	3.2	0.91
Gas	0.307	144.7	3.2	0.90
Gas	0.307	144.5	3.2	0.90
Gas	0.351	166.4	3.2	0.90

Gas	0.352	166.1	3.2	0.90
Gas	0.382	182.0	3.2	0.89
Gas	0.383	182.5	3.2	0.89
Gas	0.411	197.2	3.2	0.88
Gas	0.411	197.1	3.2	0.89
Gas	0.440	210.7	3.2	0.89
Gas	0.440	211.1	3.2	0.88
Gas	0.458	220.7	3.2	0.88
Gas	0.458	220.4	3.2	0.88
Gas	0.481	233.6	3.2	0.87
Gas	0.481	233.6	3.2	0.88
Liquid	1.440	13242.0	3.4	0.05
Liquid	1.444	13242.5	3.3	0.05
Liquid	1.550	13248.8	3.4	0.05
Liquid	1.553	13248.7	3.2	0.05
Liquid	1.744	13260.3	3.4	0.06
Liquid	1.748	13260.9	3.3	0.06
Liquid	1.842	13266.3	3.4	0.06
Liquid	1.847	13266.6	3.3	0.06
Liquid	1.905	13270.0	3.4	0.06
Liquid	1.912	13270.4	3.3	0.06
Liquid	2.014	13276.7	3.3	0.06
Liquid	2.019	13276.9	3.3	0.06
Liquid	2.100	13281.7	3.4	0.07
Liquid	2.105	13282.1	3.3	0.07
Liquid	2.242	13290.7	3.4	0.07
Liquid	2.245	13290.5	3.3	0.07
Liquid	2.466	13303.9	3.3	0.08
Liquid	2.468	13303.9	3.3	0.08
Liquid	2.981	13333.2	3.3	0.10
Liquid	2.983	13333.2	3.3	0.10
Liquid	3.478	13361.0	3.3	0.11
Liquid	3.478	13360.8	3.5	0.11
Liquid	3.961	13387.2	3.3	0.13
Liquid	3.963	13387.1	3.3	0.13
Liquid	3.970	13388.3	3.5	0.13
Liquid	4.462	13414.5	3.8	0.14
Liquid	4.464	13414.6	3.4	0.14
Liquid	5.004	13443.5	3.2	0.16
Liquid	5.005	13443.4	3.2	0.16
Liquid	5.988	13493.7	3.2	0.19
Liquid	5.990	13493.8	3.2	0.19
Liquid	6.977	13542.6	3.2	0.22

Liquid	6.980	13542.7	3.2	0.22
Liquid	7.997	13590.9	3.2	0.25
Liquid	7.999	13591.1	3.2	0.25
Liquid	9.007	13637.2	3.2	0.28
Liquid	9.009	13637.3	3.2	0.28
Liquid	10.034	13681.6	3.2	0.31
		318.19 K		
Liquid	2.917	11497.4	8.2	0.10
Liquid	2.919	11496.8	8.2	0.10
Liquid	2.954	11504.2	8.3	0.10
Liquid	2.959	11504.4	8.3	0.10
Liquid	3.053	11518.6	8.3	0.10
Liquid	3.060	11519.4	8.3	0.10
Liquid	3.156	11533.4	8.3	0.10
Liquid	3.161	11534.1	8.3	0.10
Liquid	3.233	11546.0	8.3	0.11
Liquid	3.242	11546.6	8.3	0.11
Liquid	3.332	11560.4	8.3	0.11
Liquid	3.337	11560.7	8.3	0.11
Liquid	3.412	11572.0	8.3	0.11
Liquid	3.417	11572.3	8.3	0.11
Liquid	3.504	11585.1	8.3	0.11
Liquid	3.508	11585.6	8.3	0.11
Liquid	3.592	11598.0	8.3	0.12
Liquid	3.595	11597.8	8.2	0.12
Liquid	3.697	11612.2	8.2	0.12
Liquid	3.699	11612.9	8.3	0.12
Liquid	3.793	11626.2	8.3	0.12
Liquid	3.798	11626.9	8.3	0.12
Liquid	3.865	11635.5	8.2	0.13
Liquid	3.867	11636.4	8.3	0.13
Liquid	3.966	11650.6	8.3	0.13
Liquid	3.969	11651.5	8.3	0.13
Liquid	4.098	11668.7	8.2	0.13
Liquid	4.101	11669.6	8.3	0.13
Liquid	4.167	11680.2	8.3	0.13
Liquid	4.168	11679.1	8.3	0.13
Liquid	4.392	11708.2	8.3	0.14
Liquid	4.396	11708.6	8.3	0.14
Liquid	4.548	11729.6	8.5	0.15
Liquid	4.551	11728.7	8.3	0.15
Liquid	4.775	11757.2	8.3	0.15
Liquid	4.777	11757.2	8.3	0.15

Liquid	5.092	11795.5	8.7	0.16
Liquid	5.095	11794.5	8.3	0.16
Liquid	5.394	11830.6	8.3	0.17
Liquid	5.396	11829.5	8.3	0.17
Liquid	5.691	11863.9	8.3	0.18
Liquid	5.693	11865.0	8.3	0.18
Liquid	5.964	11894.3	8.3	0.19
Liquid	5.967	11895.6	8.3	0.19
Liquid	6.498	11951.2	8.3	0.21
Liquid	6.500	11950.9	8.3	0.21
Liquid	6.984	12000.4	8.3	0.22
Liquid	6.985	11999.3	8.3	0.22
Liquid	7.505	12051.9	8.3	0.24
Liquid	7.508	12050.3	8.3	0.24
Liquid	7.998	12098.8	8.6	0.25
Liquid	8.001	12098.3	8.4	0.25
Liquid	9.003	12187.1	10.4	0.28
Liquid	9.007	12186.1	8.3	0.28
Liquid	9.995	12266.9	8.9	0.31
Liquid	9.997	12268.6	8.9	0.31
		353.00 K		
Gas	0.502	179.6	3.9	0.95
Gas	0.507	182.4	3.9	0.95
Gas	1.003	380.2	3.9	0.90
Gas	1.531	609.8	3.9	0.86
Gas	2.023	840.2	3.9	0.82
Gas	2.622	1181.2	3.9	0.76
Liquid	5.317	8967.0	3.9	0.20
Liquid	5.501	9109.8	3.9	0.21
Liquid	5.600	9173.9	3.9	0.21
Liquid	5.690	9230.5	3.9	0.21
Liquid	5.790	9288.4	3.9	0.21
Liquid	5.893	9347.4	3.9	0.21
Liquid	6.003	9404.3	3.9	0.22
Liquid	6.196	9495.2	3.9	0.22
Liquid	6.391	9581.4	3.9	0.23
Liquid	6.599	9659.3	3.9	0.23
Liquid	6.887	9765.4	4.0	0.24
Liquid	7.219	9876.6	3.9	0.25
Liquid	7.486	9952.9	3.9	0.26
Liquid	7.984	10089.7	4.0	0.27
Liquid	8.485	10214.5	4.0	0.28
Liquid	8.960	10316.0	3.9	0.30

Liquid	10.025	10521.5	4.1	0.32
59.6% CO_2 + 40.4% R1234ze(E)				
283.04 K				
Gas	0.400	211.7	2.0	0.80
Gas	0.400	212.1	2.0	0.80
Gas	0.453	242.0	2.0	0.79
Gas	0.453	241.8	2.0	0.80
Gas	0.500	270.1	2.0	0.79
Gas	0.500	270.5	2.0	0.79
Gas	0.550	309.0	2.0	0.76
Gas	0.550	308.4	2.0	0.76
Gas	0.600	375.2	2.0	0.68
Gas	0.601	374.9	2.0	0.68
Liquid	2.360	15654.2	4.0	0.06
Liquid	2.366	15654.8	4.0	0.06
Liquid	2.417	15655.2	4.0	0.07
Liquid	2.421	15655.7	3.9	0.07
Liquid	2.497	15660.8	4.0	0.07
Liquid	2.500	15661.3	3.9	0.07
Liquid	2.548	15664.2	4.0	0.07
Liquid	2.548	15664.2	3.9	0.07
Liquid	2.659	15671.6	4.0	0.07
Liquid	2.660	15671.7	3.9	0.07
Liquid	2.807	15682.5	4.0	0.08
Liquid	2.810	15682.2	4.0	0.08
Liquid	2.968	15692.7	4.0	0.08
Liquid	2.971	15693.1	3.9	0.08
Liquid	3.160	15706.3	4.0	0.09
Liquid	3.164	15706.6	3.9	0.09
Liquid	3.369	15719.7	4.1	0.09
Liquid	3.374	15720.4	3.9	0.09
Liquid	3.675	15740.5	4.1	0.10
Liquid	3.679	15740.3	4.0	0.10
Liquid	3.969	15759.8	4.1	0.11
Liquid	3.972	15760.1	3.9	0.11
Liquid	4.468	15792.5	4.4	0.12
Liquid	4.472	15792.7	4.5	0.12
Liquid	4.987	15826.0	3.9	0.13
Liquid	4.989	15826.0	3.9	0.13
Liquid	5.504	15857.4	3.9	0.15
Liquid	5.508	15858.3	3.9	0.15
Liquid	5.987	15887.2	3.9	0.16
Liquid	5.990	15887.7	3.9	0.16

Liquid	6.991	15947.2	3.9	0.19
Liquid	6.993	15947.2	3.9	0.19
Liquid	7.994	16004.8	3.9	0.21
Liquid	7.996	16005.3	3.9	0.21
Liquid	9.003	16060.6	3.9	0.24
Liquid	9.004	16061.2	3.9	0.24
Liquid	10.051	16116.2	3.9	0.27
Liquid	10.060	16115.9	3.9	0.27
		298.33 K		
Gas	1.001	477.4	14.6	0.85
Gas	1.001	478.1	14.6	0.84
Gas	1.025	499.5	14.6	0.83
Gas	1.026	496.2	14.6	0.83
Gas	1.061	527.4	14.6	0.81
Gas	1.062	526.5	14.6	0.81
Gas	1.093	551.6	14.6	0.80
Gas	1.093	550.2	14.6	0.80
Gas	1.123	574.4	14.6	0.79
Gas	1.123	574.0	14.6	0.79
Gas	1.150	594.6	14.6	0.78
Gas	1.150	594.5	14.6	0.78
Liquid	3.117	13931.3	14.6	0.09
Liquid	3.117	13931.0	14.7	0.09
Liquid	3.254	13950.0	14.7	0.09
Liquid	3.259	13950.1	14.6	0.09
Liquid	3.300	13957.9	14.7	0.10
Liquid	3.303	13957.6	14.6	0.10
Liquid	3.413	13973.8	14.7	0.10
Liquid	3.418	13973.8	14.7	0.10
Liquid	3.562	13995.9	14.7	0.10
Liquid	3.565	13995.9	14.6	0.10
Liquid	3.584	14006.5	14.7	0.10
Liquid	3.589	14006.9	14.7	0.10
Liquid	3.620	14014.7	14.7	0.10
Liquid	3.624	14014.2	14.6	0.10
Liquid	3.629	14020.8	14.7	0.10
Liquid	3.641	14022.6	14.7	0.10
Liquid	3.677	14028.0	14.7	0.11
Liquid	3.681	14028.2	14.6	0.11
Liquid	3.790	14044.3	14.7	0.11
Liquid	3.796	14045.1	14.7	0.11
Liquid	3.963	14064.5	14.6	0.11
Liquid	3.966	14065.3	14.6	0.11

Liquid	4.130	14085.2	14.7	0.12
Liquid	4.134	14084.9	14.6	0.12
Liquid	4.341	14112.7	14.7	0.12
Liquid	4.346	14113.2	14.7	0.12
Liquid	4.688	14153.5	14.7	0.13
Liquid	4.692	14153.5	14.6	0.13
Liquid	4.992	14189.1	14.7	0.14
Liquid	4.996	14188.5	14.7	0.14
Liquid	5.480	14243.0	14.7	0.16
Liquid	5.484	14243.5	14.8	0.16
Liquid	5.998	14299.0	14.9	0.17
Liquid	6.003	14299.4	14.8	0.17
Liquid	6.494	14350.3	14.9	0.18
Liquid	6.499	14350.1	14.7	0.18
Liquid	6.989	14399.9	14.7	0.20
Liquid	6.991	14399.6	14.6	0.20
Liquid	8.002	14495.9	14.7	0.22
Liquid	8.002	14496.8	14.6	0.22
Liquid	9.034	14589.1	14.7	0.25
Liquid	9.038	14589.6	14.6	0.25
Liquid	10.015	14670.8	14.6	0.28
Liquid	10.018	14671.9	14.6	0.28
		318.07 K		
Gas	1.502	652.5	6.6	0.87
Gas	1.700	756.6	6.6	0.85
Gas	1.700	756.3	6.6	0.85
Gas	1.803	816.9	6.6	0.83
Gas	1.803	816.8	6.6	0.83
Gas	1.901	874.3	6.6	0.82
Gas	1.902	874.3	6.6	0.82
Gas	1.951	900.7	6.6	0.82
Gas	1.952	901.3	6.6	0.82
Gas	1.952	902.3	6.6	0.82
Gas	2.005	932.0	6.6	0.81
Gas	2.006	932.3	6.6	0.81
Gas	2.050	959.5	6.6	0.81
Gas	2.052	960.1	6.6	0.81
Gas	2.081	977.4	6.6	0.81
Gas	2.082	977.9	6.6	0.80
Gas	2.112	996.8	6.6	0.80
Gas	2.113	997.1	6.6	0.80
Liquid	4.693	12435.1	6.6	0.14
Liquid	4.693	12435.4	6.6	0.14

Liquid	4.804	12471.6	6.7	0.15
Liquid	4.804	12470.1	6.6	0.15
Liquid	4.868	12488.5	6.7	0.15
Liquid	4.868	12488.6	6.7	0.15
Liquid	5.002	12501.3	6.7	0.15
Liquid	5.004	12500.5	6.6	0.15
Liquid	5.181	12547.7	6.7	0.16
Liquid	5.184	12548.9	6.7	0.16
Liquid	5.404	12603.1	6.6	0.16
Liquid	5.407	12602.5	6.7	0.16
Liquid	5.719	12676.7	6.7	0.17
Liquid	5.720	12676.8	6.6	0.17
Liquid	5.983	12735.9	6.6	0.18
Liquid	5.984	12735.1	6.7	0.18
Liquid	6.503	12846.1	6.7	0.19
Liquid	6.508	12846.5	6.8	0.19
Liquid	6.998	12940.9	6.7	0.20
Liquid	7.000	12940.9	6.7	0.20
Liquid	7.513	13033.5	6.8	0.22
Liquid	7.515	13033.3	6.7	0.22
Liquid	8.023	13121.2	6.8	0.23
Liquid	8.027	13120.4	6.7	0.23
Liquid	8.990	13271.5	7.6	0.26
Liquid	8.995	13270.7	7.8	0.26
Liquid	10.018	13410.3	6.8	0.28
Liquid	10.021	13409.5	7.5	0.28
		353.02 K		
Supercritical	0.227	77.3	7.5	1.00
Supercritical	0.227	77.8	7.5	1.00
Supercritical	1.010	367.9	7.5	0.93
Supercritical	1.010	367.2	7.5	0.94
Supercritical	2.032	772.9	7.5	0.90
Supercritical	2.033	778.0	7.5	0.89
Supercritical	3.019	1233.8	7.5	0.83
Supercritical	3.026	1236.8	7.5	0.83
Supercritical	3.650	1552.5	7.5	0.80
Supercritical	3.652	1553.5	7.5	0.80
Supercritical	4.079	1896.4	7.5	0.73
Supercritical	4.080	1897.0	7.5	0.73
Supercritical	4.581	2450.0	7.5	0.64
Supercritical	4.581	2458.1	7.5	0.63
Supercritical	5.090	3055.5	7.5	0.57
Supercritical	5.235	3210.6	7.5	0.56

Supercritical	5.616	3806.1	7.5	0.50
Supercritical	5.735	4042.8	7.5	0.48
Supercritical	5.920	4439.3	7.5	0.45
Supercritical	6.063	4745.8	7.5	0.44
Supercritical	6.121	4876.5	7.5	0.43
Supercritical	6.211	5086.0	7.5	0.42
Supercritical	6.251	5180.4	7.5	0.41
Supercritical	6.305	5298.9	7.5	0.41
Supercritical	6.399	5545.6	7.5	0.39
Supercritical	6.485	6033.4	7.5	0.37
Supercritical	6.578	6319.8	7.5	0.35
Supercritical	6.622	6433.5	7.5	0.35
Supercritical	6.687	6622.6	7.5	0.34
Supercritical	6.893	7247.8	7.5	0.32
Supercritical	7.105	7773.1	7.5	0.31
Supercritical	7.328	8120.4	7.5	0.31
Supercritical	7.674	8510.9	7.5	0.31
Supercritical	8.078	8918.3	7.5	0.31
Supercritical	8.513	9315.3	7.5	0.31
Supercritical	8.995	9685.6	7.5	0.32
Supercritical	9.505	10010.4	7.5	0.32
Supercritical	10.015	10274.3	7.5	0.33
79.4% CO_2 + 20.6% R1234ze(E)				
283.12 K				
Gas	1.252	563.4	6.1	0.94
Gas	1.252	563.1	6.1	0.94
Gas	1.279	575.9	6.1	0.94
Gas	1.279	575.9	6.1	0.94
Gas	1.304	590.2	6.1	0.94
Gas	1.304	590.2	6.1	0.94
Liquid	3.272	17147.4	6.1	0.08
Liquid	3.272	17147.6	6.1	0.08
Liquid	3.280	17139.8	6.1	0.08
Liquid	3.281	17140.5	6.1	0.08
Liquid	3.299	17153.3	6.1	0.08
Liquid	3.300	17153.6	6.1	0.08
Liquid	3.321	17158.0	6.1	0.08
Liquid	3.322	17158.6	6.1	0.08
Liquid	3.434	17177.7	6.1	0.08
Liquid	3.437	17177.6	6.1	0.09
Liquid	3.658	17207.7	6.1	0.09
Liquid	3.663	17208.8	6.1	0.09
Liquid	3.850	17232.7	6.1	0.09

Liquid	3.852	17232.5	6.1	0.09
Liquid	3.965	17247.0	6.1	0.10
Liquid	3.967	17247.4	6.1	0.10
Liquid	4.489	17300.0	6.1	0.11
Liquid	4.515	17303.3	6.1	0.11
Liquid	5.045	17345.3	6.1	0.12
Liquid	5.055	17345.7	6.1	0.12
Liquid	5.529	17402.4	6.1	0.13
Liquid	5.533	17403.1	6.1	0.14
Liquid	6.023	17462.0	6.1	0.15
Liquid	6.027	17461.7	6.1	0.15
Liquid	7.001	17556.8	6.1	0.17
Liquid	7.007	17556.9	6.1	0.17
Liquid	7.983	17662.6	6.1	0.19
Liquid	7.984	17664.0	6.1	0.19
Liquid	10.180	17874.3	6.1	0.24
Liquid	10.180	17874.1	6.1	0.24
		293.17 K		
Gas	1.601	795.2	6.2	0.83
Gas	1.602	795.2	6.2	0.83
Gas	1.652	823.0	6.2	0.82
Gas	1.652	822.2	6.2	0.82
Gas	1.704	850.6	6.2	0.82
Gas	1.704	852.4	6.2	0.82
Gas	1.725	864.7	6.2	0.82
Gas	1.725	864.4	6.2	0.82
Gas	1.750	879.3	6.2	0.82
Gas	1.750	878.6	6.2	0.82
Gas	1.769	890.8	6.2	0.81
Gas	1.769	891.3	6.2	0.81
Gas	1.794	906.3	6.2	0.81
Gas	1.795	906.1	6.2	0.81
Gas	1.828	932.0	6.2	0.80
Gas	1.829	932.7	6.2	0.80
Liquid	4.090	16263.5	6.8	0.10
Liquid	4.099	16265.1	6.3	0.10
Liquid	4.109	16268.0	6.6	0.10
Liquid	4.116	16269.5	6.2	0.10
Liquid	4.128	16271.0	6.3	0.10
Liquid	4.133	16271.6	6.2	0.10
Liquid	4.152	16276.2	6.3	0.10
Liquid	4.157	16276.6	6.2	0.10
Liquid	4.182	16282.2	6.2	0.11

Liquid	4.183	16282.1	6.2	0.11
Liquid	4.754	16390.0	6.2	0.12
Liquid	4.762	16391.5	6.4	0.12
Liquid	4.858	16406.7	6.2	0.12
Liquid	4.862	16407.9	6.3	0.12
Liquid	5.507	16520.0	6.2	0.14
Liquid	5.508	16520.2	6.3	0.14
Liquid	6.012	16603.5	6.2	0.15
Liquid	6.015	16603.6	6.2	0.15
Liquid	6.469	16675.7	6.2	0.16
Liquid	6.472	16676.1	6.2	0.16
Liquid	6.990	16754.7	6.2	0.17
Liquid	6.992	16754.2	6.2	0.17
Liquid	8.002	16899.5	6.2	0.19
Liquid	8.004	16899.0	6.2	0.19
Liquid	9.015	17031.9	6.2	0.22
Liquid	9.017	17031.9	6.2	0.22
Liquid	10.099	17161.3	6.2	0.24
Liquid	10.100	17162.5	6.2	0.24
Liquid	10.102	17163.2	6.2	0.24
		308.26 K		
Gas	2.600	1272.8	42.7	0.80
Gas	2.601	1272.3	42.7	0.80
Gas	2.682	1338.6	42.7	0.78
Gas	2.682	1336.5	42.7	0.78
Gas	2.740	1381.3	42.7	0.77
Gas	2.741	1380.3	42.7	0.77
Gas	2.779	1403.3	42.7	0.77
Gas	2.780	1403.1	42.7	0.77
Gas	2.798	1410.0	42.7	0.77
Gas	2.799	1409.8	42.7	0.77
Gas	2.822	1421.9	42.7	0.77
Gas	2.822	1422.2	42.7	0.77
Gas	2.839	1430.0	42.7	0.77
Gas	2.840	1430.2	42.7	0.77
Gas	2.857	1441.6	42.7	0.77
Gas	2.859	1442.1	42.7	0.77
Gas	2.894	1460.8	42.7	0.77
Gas	2.894	1460.9	42.7	0.77
Liquid	5.503	14377.3	42.7	0.15
Liquid	5.505	14378.6	42.7	0.15
Liquid	5.520	14384.5	42.7	0.15
Liquid	5.522	14384.9	42.7	0.15

Liquid	5.534	14396.6	42.7	0.15
Liquid	5.545	14399.6	42.7	0.15
Liquid	5.550	14410.0	42.7	0.15
Liquid	5.557	14410.7	42.7	0.15
Liquid	5.573	14418.9	42.7	0.15
Liquid	5.576	14424.6	42.7	0.15
Liquid	5.581	14424.7	42.7	0.15
Liquid	5.592	14428.6	42.7	0.15
Liquid	5.602	14425.3	42.7	0.15
Liquid	5.612	14433.3	42.7	0.15
Liquid	5.648	14441.3	42.7	0.15
Liquid	5.652	14441.7	42.7	0.15
Liquid	5.683	14474.2	42.8	0.15
Liquid	5.695	14475.5	42.7	0.15
Liquid	5.834	14537.4	42.8	0.16
Liquid	5.843	14540.1	42.7	0.16
Liquid	5.988	14617.6	42.8	0.16
Liquid	5.997	14619.2	42.8	0.16
Liquid	6.186	14689.3	42.8	0.16
Liquid	6.194	14689.9	42.7	0.16
Liquid	6.500	14804.4	42.8	0.17
Liquid	6.509	14803.9	42.7	0.17
Liquid	6.993	14969.1	42.9	0.18
Liquid	7.001	14969.3	42.8	0.18
Liquid	7.495	15116.8	42.9	0.19
Liquid	7.499	15115.0	42.9	0.19
Liquid	8.003	15259.8	52.4	0.20
Liquid	8.008	15257.8	48.1	0.20
Liquid	8.928	15483.8	42.7	0.23
Liquid	8.931	15481.1	42.8	0.23
Liquid	10.348	15765.8	42.7	0.26
Liquid	10.349	15766.3	42.7	0.26
		333.03 K		
Supercritical	4.009	1862.4	4.3	0.78
Supercritical	4.015	1870.9	4.3	0.77
Supercritical	4.519	2293.5	4.3	0.71
Supercritical	4.520	2293.3	4.3	0.71
Supercritical	5.024	2666.5	4.3	0.68
Supercritical	5.028	2673.7	4.3	0.68
Supercritical	5.301	2961.8	4.3	0.65
Supercritical	5.303	2962.8	4.3	0.65
Supercritical	5.641	3409.7	4.3	0.60
Supercritical	5.644	3417.6	4.3	0.60

Supercritical	5.712	3521.2	4.3	0.59
Supercritical	5.714	3523.9	4.3	0.59
Supercritical	5.818	3684.0	4.4	0.57
Supercritical	5.828	3699.8	4.3	0.57
Supercritical	5.884	3780.4	4.3	0.56
Supercritical	5.888	3785.8	4.4	0.56
Supercritical	5.929	3849.8	4.3	0.56
Supercritical	5.934	3856.9	4.3	0.56
Supercritical	6.013	3978.9	4.3	0.55
Supercritical	6.014	3980.4	4.3	0.55
Supercritical	6.212	4344.7	4.3	0.52
Supercritical	6.429	4632.0	4.3	0.50
Supercritical	6.622	4924.2	4.3	0.49
Supercritical	6.835	5507.7	4.4	0.45
Supercritical	6.945	5846.0	4.4	0.43
Supercritical	8.270	9800.9	4.5	0.30
Supercritical	8.603	10370.2	5.2	0.30
Supercritical	8.994	11000.3	4.4	0.30
Supercritical	9.496	11583.6	4.4	0.30
Supercritical	10.016	12018.7	4.5	0.30

The adjusted β_T and γ_T on VLE data measured by Wang et al. are presented in Table 7. The values of the objective function (OF1) are also presented. As an example, the plot of β_T in function of the temperature is shown in the figure 3. It can be seen from the figure that there is a discontinuity of β_T when the temperature is above the critical temperature of CO_2.

[Table 7]

Table 7: Adjusted β_T and γ_T and its objective function

T(K)	β_T	γ_T	OF1
283.32	0.982038	1.005529	0.022
293.15	0.991769	1.004044	0.010
298.15	0.994880	1.006619	0.011
308.13	0.983614	1.004744	0.010
318.11	0.986412	0.998124	0.014
333.01	0.986650	0.994529	0.010
353.02	1.006391	0.991355	0.004

[Figure 3]

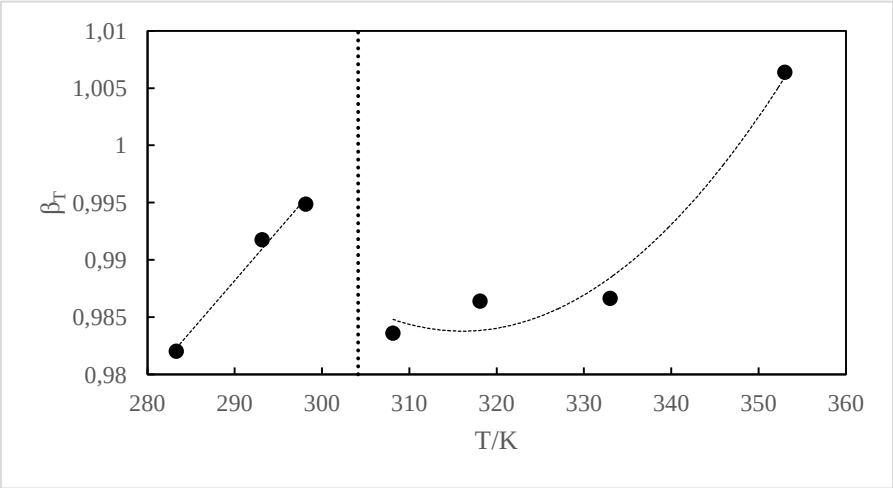

Figure 3 Variation of β_T as a function of the temperature

The adjusted β_v and γ_v, as well as the objective function is presented in Table 8.

[Table 8]

Table 8: Adjusted β_v and γ_v and objective function OF2.

Composition	T/K	β_T	γ_T	β_v	γ_v	OF2
21.3% CO_2 + 78.7% R1234ze(E)	318.17	0.986412	0.998124	1.044502	1.065207	0.0032
	333.01	0.986650	0.994529	1.053472	1.061821	0.0035
	353.05	1.006391	0.991355	1.076660	0.973199	0.0056
40.0% CO_2 + 60.0% R1234ze(E)	283.09	0.982038	1.005529	1.065055	1.041867	0.0036
	318.19	0.986412	0.998124	1.075621	1.016056	0.0001
	353.00	1.006391	0.991355	1.093223	0.969159	0.0130
59.6% CO_2 + 40.4% R1234ze(E)	283.04	0.982038	1.005529	1.017762	0.935516	0.0129
	298.33	0.99488	1.006619	1.012940	1.029388	0.0053
	318.07	0.986412	0.998124	1.030651	0.999307	0.0007
	353.02	1.006391	0.991355	1.051448	1.242321	0.0078
79.4% CO_2 + 20.6% R1234ze(E)	283.12	0.982038	1.005529	1.065550	0.959538	0.0049
	293.17	0.991769	1.004044	1.044714	0.979503	0.0038
	308.26	0.983614	1.004744	1.042739	0.966820	0.0017
	333.03	0.986650	0.994529	1.028689	1.193879	0.0042

As it can be seen in Table 8, if the temperature is close to, even higher than the critical temperature, the objective function is larger. It is probably due to the fact that experimental data are less stable and the adjustment is more difficult.

Figure 4 presents the phase diagrams and the comparison with experimental data obtained by Wang et al. [8]. It can be seen that the data are well correlated for temperature lower than the critical temperature of CO_2. For temperature higher than the critical temperature of CO_2, the model is not able to represent correctly the data close to the mixture critical point. This point was previously highlighted by Xie et al. [9]. For binary systems, it is not uncommon for multiparametric or molecular models to have difficulties to correctly represent VLE at temperatures below and above the critical temperatures of the most volatile component. We have plotted on figure 4 the results obtained with the CP-PC-SAFT EoS [24] model. The molecular parameters (Table 9) are solved at the critical points and binary interaction parameter $k_{12} = 0$. We can conclude that SAFT model predicts the VLE data with similar and even superior accuracy than the Fundamental Helmholtz energy based EoS.

[Table 9]

Table 9: Parameters of the CP-PC-SAFT EoS [24].

Component	*m*	*σ (A)*	*ε/k (K)*
CO_2	2.03351	2.81786	163.49073
R1234ze[E]	2.95808	3.33702	175.47269

[Figure 4]

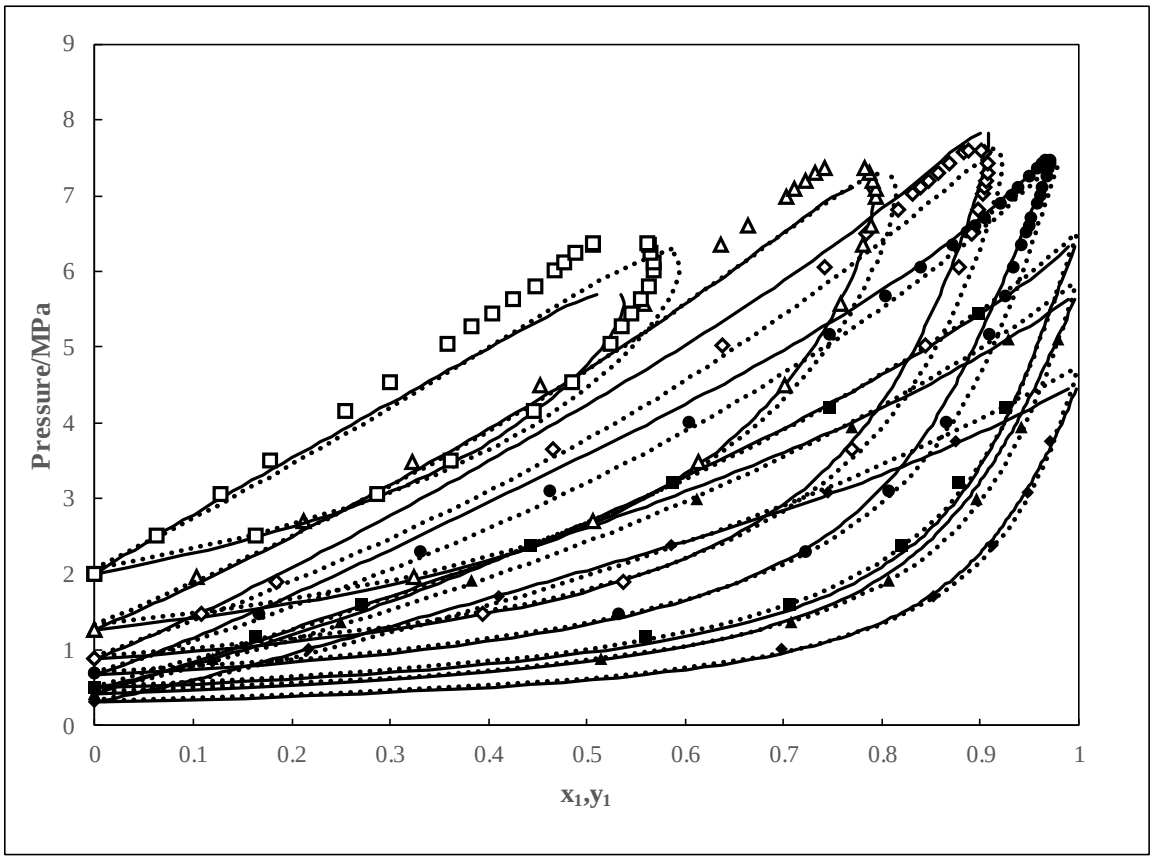

Figure 4 P-x-y Diagram of the CO_2 (1) + R1234ze(E) (2) binary systems. (♦) 283.32K (exp), (▲) 293.15K (exp), (■) 298.15K (exp), (●) 308.13K (exp), (◊) 318.11K (exp), (△) 333.01K (exp), (□) 353.02K (exp). Helmholtz Equation of state (solid line), CP-PC-SAFT EoS (dashed line).

The experimental and calculation data of P-ρ diagram with adjusted β_v,γ_v,β_T, and $\gamma_T$at experimental temperatures are plotted in Figure 2. The experimental and calculation data of compressibility factor vs pressure (Z-P) diagram with adjustedβ_v, γ_v, β_T, and γ_T at experimental temperature are plotted in Figures 5, where the squares denote the experimental data, and the full line represents the results calculated by model using Helmholtz Eos in Matlab®:

It can be seen in the figures that the prediction model calculated by Matlab® with adjusted parameters have higher agreement on experimental data than that calculated by REFPROP

10.0 especially for the liquid phase. However, when the temperature is close to the critical temperature or even at supercritical phase, the model over predict the experimental data. We have also compared the density prediction obtained with the predictive CP-PC-SAFT EoS [24] model with our experimental data. The deviations between calculation value and experimental value, MRDρ and BIASρ on densities are defined by Eqs (23-24).

$$MRDU = \frac{100}{N_{data}} \sum \left| \frac{U_{cal} - U_{exp}}{U_{exp}} \right| \quad (23)$$

The BIAS is defined by:

$$BIASU = \frac{100}{N_{data}} \sum \left(\frac{U_{cal} - U_{exp}}{U_{exp}} \right) \quad (24)$$

The deviations in between calculation value and experimental value, MRD and BIAS are presented by Table 10 for the three models. In general, the deviations are smaller with the Helmholtz equation of state and they became larger when the temperature is close to the critical temperature or even at supercritical phase. It appears also that deviations are slightly lower with the CP-PC-SAFT than with the Peng Robinson Equation of state particularly at low temperature, far from the mixture critical point. For the low temperature, the deviation is mainly from the vapor phase, while at high temperature, the deviation is mainly from the liquid phase.

In order to improve the prediction around and above the mixture critical point, it is necessary to have more experimental data. Another possibility is to take into account the departure function and adjust corresponding parameters on more mixture density or speed of sound data.

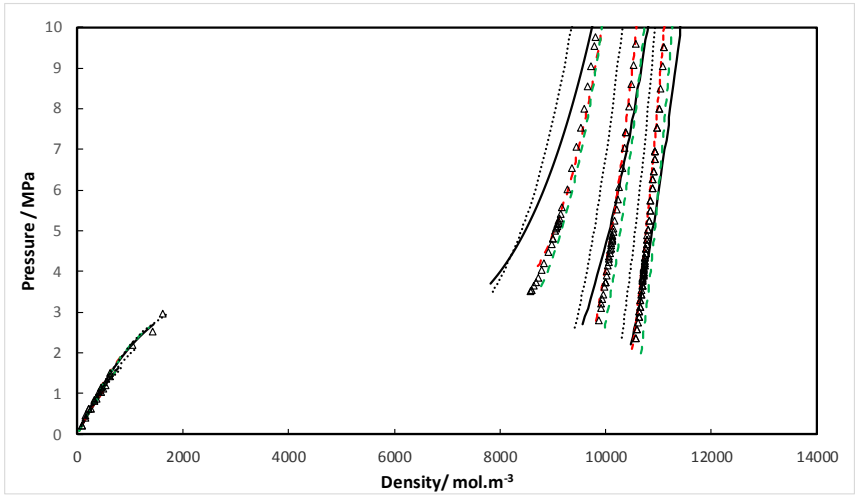

CO_2/R1234ze(E) (21.3/78.7)

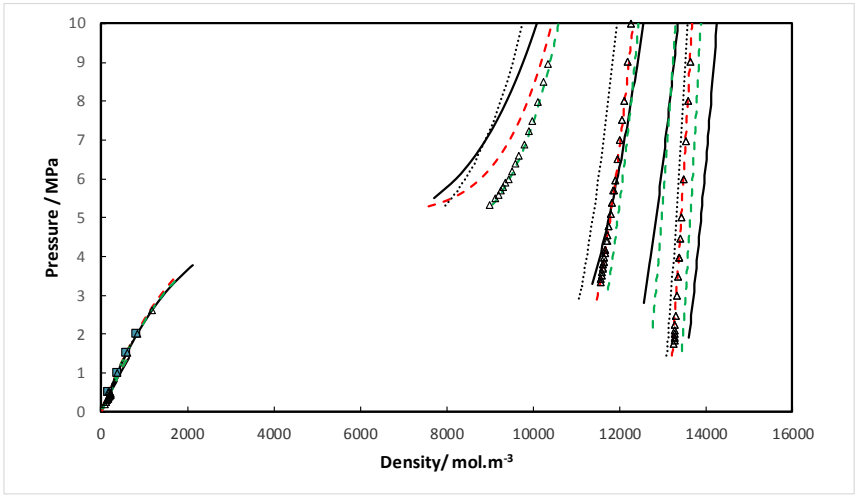

CO_2/R1234ze(E) (40/60)

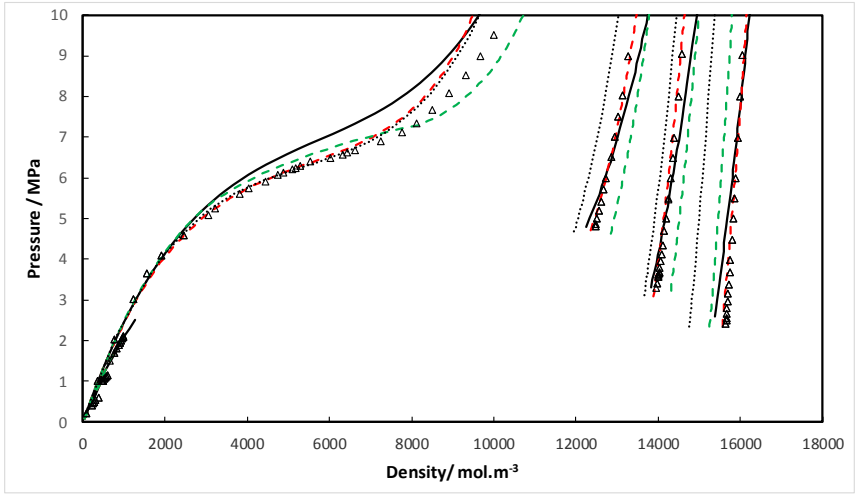

CO_2/R1234ze(E) (59.6/40.4)

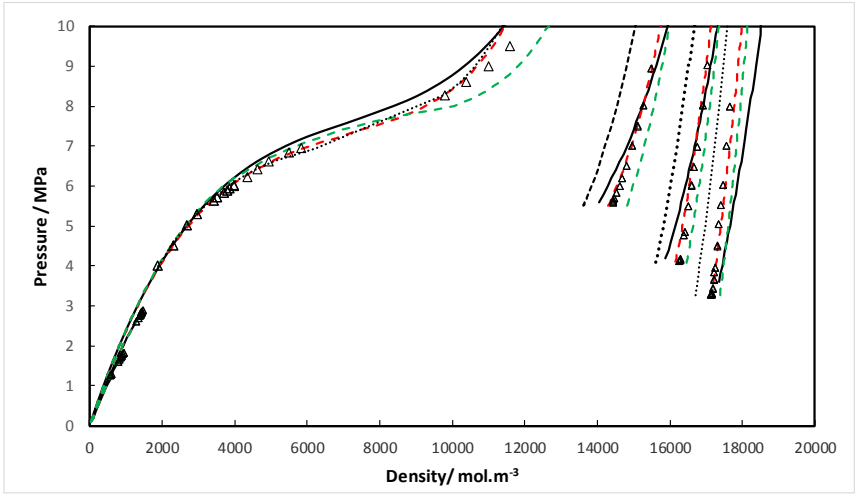

CO_2/R1234ze(E) (79.4/20.6)

Figure 2: Comparison between experimental data and predictions using PR EoS model developed by Wang et al.[8] (solid line), REFPROP 10.0 (dotted green line), Helmholtz Equation of state (dotted red line), CP-PC-SAFT EoS (black dashed line).

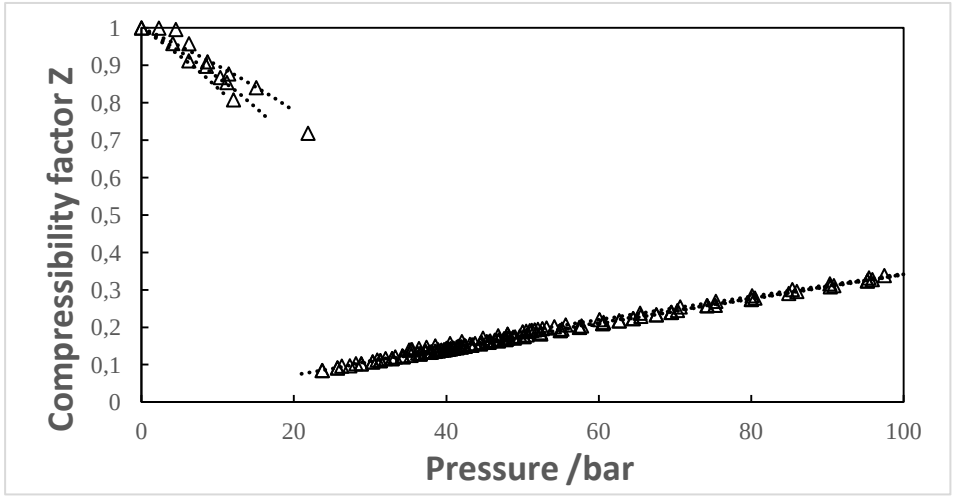

CO_2/R1234ze(E) (21.3/78.7)

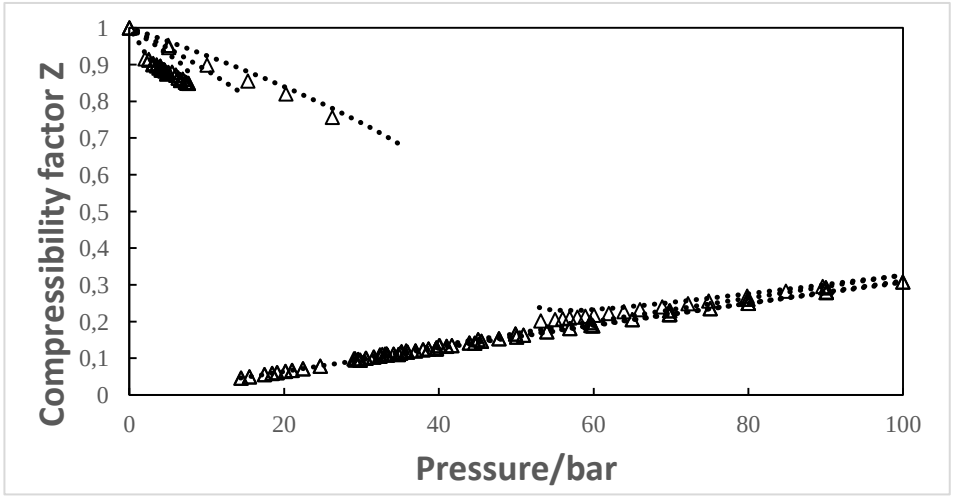

CO_2/R1234ze(E) (40/60)

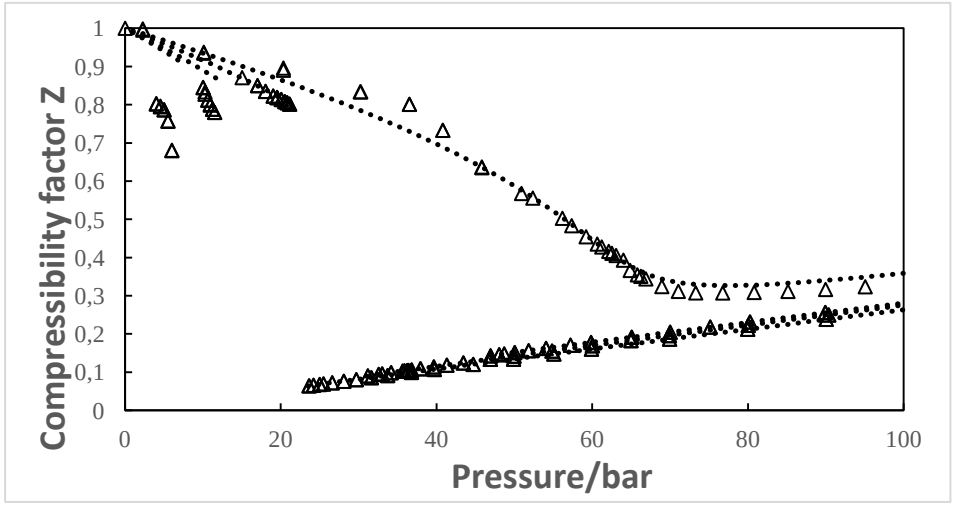

CO_2/R1234ze(E) (59.6/40.4)

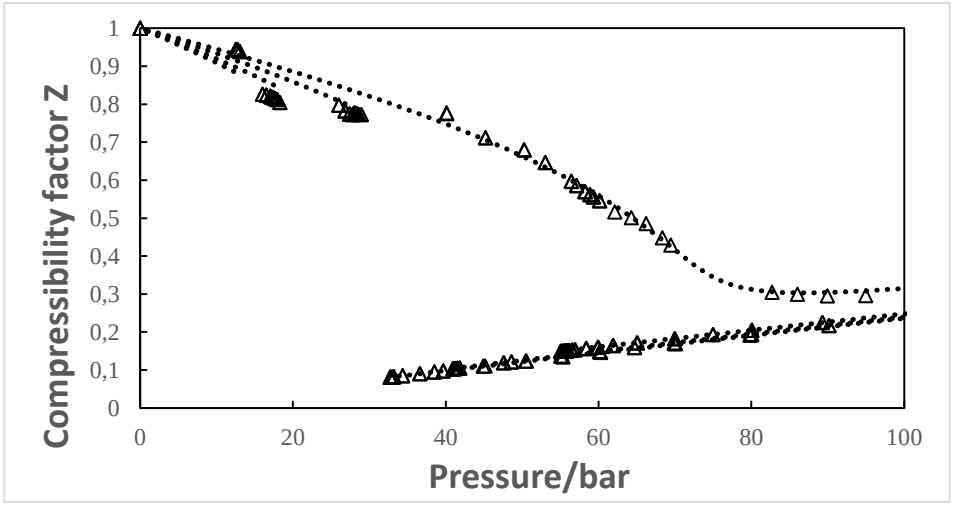

CO_2/R1234ze(E) (79.4/20.6)

Figure 5: Comparison between experimental data and predictions using Helmholtz EoS.

[Table 10]

Table 10: MRDρ and BIAS using the Helmholtz EoS, PR EoS and CP-PC-SAFT EoS.

		Helmholtz EoS [21]		Peng-Robinson EoS [18]		CP-PC-SAFT EoS [24]	
Composition	**T(K)**	**MRDρ /%**	**BIASρ/ %**	**MRDρ /%**	**BIASρ/ %**	**MRDρ /%**	**BIASρ/ %**
21.3% CO_2 + 78.7% R1234ze(E)	318.17	1.26	-0.84	0.92	-0.83	3.20	-2.97
	333.01	1.20	-0.55	1.57	0.38	3.95	-3.85
	353.05	1.31	-0.62	4.83	4.33	6.26	-5.76
40.0% CO_2 + 60.0% R1234ze(E)	283.09	1.51	-1.51	10.5	6.78	2.38	-2.38
	318.19	0.12	0.00	0.97	0.18	3.41	-3.41
	353.00	4.77	-4.77	8.50	8.38	7.49	-7.49
59.6% CO_2 + 40.4% R1234ze(E)	283.04	4.17	-4.12	10.5	10.7	8.19	-8.19
	298.33	2.00	-2.00	2.43	1.92	3.46	-3.46
	318.07	0.38	-0.24	1.15	-0.44	2.38	-2.38
	353.02	3.56	-0.54	10.7	8.68	3.21	-0.75
79.4% CO_2 + 20.6% R1234ze(E)	283.12	1.35	1.35	26.1	21.3	2.87	-0.92
	293.17	1.76	-1.76	2.02	1.82	4.14	-4.14
	308.26	0.93	-0.90	1.22	0.94	4.20	-4.20
	333.03	1.92	-0.36	4.85	4.28	2.61	-1.17

5 Conclusion

The densities of CO_2-R1234ze(E) binary mixture were measured using VTD densitometer, Anton Paar DMA 512, in the gas, liquid and supercritical phases. The densitometer were first calibrated using pure CO_2 and the FPMC calibration technique. Then, the densities of four binary mixtures were measured at temperatures of 283.32, 293.15, 298.15, 308.13, 318.11, 333.01 and 353.02 K. The overall average uncertainty of the measured densities with the confidence level of 95% was 0.2% or 0.4 kg/m^3. The measured densities were employed to evaluate the prediction of the PR cubic EoS using the Wong Sandler mixing rules involving the NRTL activity coefficient model developed based on the existing VLE data (Wang et al. [8]). It appears that this model is accurate for the prediction of VLE but not so accurate for the prediction of densities. A fundamental Helmholtz equation of state like the one used in

REFPROP was considered. The parameters were adjusted on both VLE and density data. Using this model, we can predict correctly the phase diagram and calculate the densities of the four mixtures studied (the maximum of MRDρ is 4.77%). Also, a molecular predictive thermodynamic model, CP-PC-SAFT model, was also tested. It gives a better prediction than the fundamental Helmholtz equation of state concerning the phase diagram and better density prediction than the one calculated by the Peng-Robinson Equation of state.

6 Acknowledgement

MINES ParisTech and Shanghai Jiao Tong University (SPEIT) are acknowledged for funding Y. Fu's internship.

7 References

[1] United Nations. Montreal Protocol on Substances that Deplete the Ozone Layer (with annex). Concluded at Montreal on 16 September 1987. Montreal: United Nations, 1987.

[2] United Nations. Kyoto Protocoltothe United Nations Framework Conventionon Climate Change. Montreal: United Nations, 1998.

[3] Anonymous. Regulation (EU) No 517/2014 ofthe European Parliamentandofthe Council of 16 April 2014 on fluorinated greenhouse gases and repealing Regulation (EC) No 842/2006. Official Journal of European Union, 2014.

[4] UNEP. The Kigali Amendment to the Montreal Protocol: HFC Phase-down. Kigali: Ozon actionFact Sheet, 2016.

[5] Qiu, J., Zhang, H., Qi, Y., Wang, X., Yu, X. 2015. A study on new refrigerant R1234ze(E) and its mixture Int. J. Ref., 36, 9-16.

[6] Wu, Y. 2015. Refrigeration principle and equipment, Shanxi: Xi'an Jiaotong University press.

[7] Juntarachat, N., Valtz, A., Coquelet, C., Privat, R., Jaubert, J.N. 2014. Experimental measurements and correlation of vaporeliquid equilibrium and critical data for the CO_2 + R1234yf and CO_2 + R1234ze (E) binary mixtures. Int. J. Refrig., 47, 141-152.

[8] Wang, S., Fauve, R., Coquelet, C., Valtz, A., Houriez, C., Artola, P., El-Ahmar, E., Rousseau, B., Hu. H. 2019. Vapor–liquid equilibrium and molecular simulation data for carbon dioxide(CO2) +trans-1,3,3,3-tetrafluoroprop-1-ene(R-1234ze(E)) mixture at temperatures from 283.32 to 353.02K and pressures up to 7.6MPa, Int. J. Refrig., 98, 362-371.

[9] Xie, J., Valtz, A., Coquelet, C., Hu, H. 2019. Utilization of CO2 and R1234ze(E) as refrigerant: determination of mixture volumetric properties at the vicinity of critical point, ICR 2019, Montreal.

[10] Coquelet, C., Ramjugernath, D., Madani, H., Valtz, A., Naidoo, P., Meniai, A.H. 2010, Experimental Measurement of Volumetric Properties and Modelling of Critical Properties for Pure Hexafluoropropylene, J. Chem. Eng. Data, 55, 2093-2099

[11] Nazeri, M., Chapoy, A., Valtz, A., Coquelet, C., Tohidi, B. 2016. Densities and derived thermophysical properties of the 0.9505 CO2 + 0.0495 H2S mixture from 273 K to 353 K and pressures up to 41 MPa, Fluid Phase Equilib, 423, 156-171

[12] Lemmon, E. W., Bell, I., Huber, M.L., McLinden, M.O. 2018. NIST Standard Reference Database 23: Reference Fluid Thermodynamic and Transport Properties-REFPROP, Version 10.0, National Institute of Standards and Technology.

[13] Bouchot, C., Richon, D. 2001. An enhanced method to calibrate vibrating tubedensimeters, Fluid Phase Equilib., vol. 191 (1–2), 189–208.

[14] Khalil, W., Coquelet, C., Richon, D. 2007 High-Pressure Vapor−Liquid Equilibria, Liquid Densities, and Excess Molar Volumes for the Carbon Dioxide + 2-Propanol System from (308.10 to 348.00) K, J. Chem. Eng. Data, 52 (5), 2032–2040.

[15] Bouchot, C., Richon, D. 1998. Direct Pressure−Volume−Temperature and Vapor−Liquid Equilibrium Measurements with a Single Equipment Using a Vibrating Tube Densimeter up to 393 K and 40 MPa: Description of the Original Apparatus and New Data, Ind. Eng. Chem. Res., 37 (8), 3295–3304.

[16] Span, R., Wagner, W. 1996. A New Equation of State for Carbon Dioxide Covering the Fluid Region from the Triple-Point Temperature to 1100 K at Pressures up to 800 MPa. J. Phys. Chem. Ref. Data, 25 (6), 1509–1596.

[17] Nazeri, M., Chapoy, A., Valtz, A., Coquelet, C., Tohidi, B. 2016. Densities and derived thermophysical properties of the 0.9505 CO_2+0.0495 H_2S mixture from 273 K to 353 K and pressures up to 41 MPa, Fluid Phase Equilib., 423, 156–171.

[18] Peng, D.-Y., Robinson, D.B., 1976. A new two-constant equation of state, Ind. Eng. Chem. Fund., 15 (1), 59-64.

[19] Wong, D. S. H., Sandler, S.I. 1992. A theoretically correct mixing rule for cubic equations of state, AIChE J., 38, (5), 671-680.

[20] Renon, H., J. M. Prausnitz, J.M. 1968. Local compositions in thermodynamic excess functions for liquid mixtures, AIChE J., 14 (1), 135-144.

[21] Kunz, O., Wagner, W. 2012. The GERG-2008 Wide-Range Equation of State for Natural Gases and Other Mixtures: An Expansion of GERG-2004, J. Chem. Eng. Data, 57(11), 3032-3091.

[22] McLinden, M. O., Thol, M., Lemmon, E.W. 2010. Thermodynamic Properties of trans-1,,3,3,-tetrafluoropropene [R1234ze(E)]: Measurements of Density and Vapor Pressure and a Comprehensive Equation of State, International Refrigeration and Air Conditioning Conference, Purdue, 1-9.

[23] Herrig, S. 2018. New Helmholtz-Energy Equations of State for Pure Fluids and CCS-Relevant Mixtures, Bochum Ruhr University.

[24] Polishuk, I., 2014. Standardized critical point-based numerical solution of statistical association fluid theory parameters: the perturbed chain-statistical association fluid theory equation of state revisited, Ind. Eng. Chem. Res., 53 (36), 14127-14141.

List of figures

List of Tables